View metadata, citation and similar papers at core.ac.uk

brought to you by CORE

provided by Directory of Open Access Journals

IPPI

Polyolefins Journal, Vol. 4, No. 1 (2017)
DOI: 10.22063/poj.2016.1375

ORIGINAL PAPER

Preparation of high performance PP/ reduced graphene oxide nanocomposites through a combined in situ polymerization and masterbatch method

He-Xin Zhang[1,2], Seung-Ri Lee[1], Dong-Ho Lee[1], Xue-Quan Zhang[2], Keun-Byoung Yoon[*1]

[1]Department of Polymer Science and Engineering, Kyungpook National University, Korea

[2]Key Lab. of Synthetic Rubber, Changchun Institute of Applied Chemistry, Chinese Academy of Science, China

Received: 26 April 2016, Accepted: 31 July 2016

ABSTRACT

Despite the great potential of graphene as a nanofiller, achieving homogeneous dispersion remains the key challenge for effectively reinforcing polyolefin (such as polyethylene (PE) and polypropylene (PP)) nanocomposites. Therefore, in this research, we report a facile combined in situ polymerization and masterbatch method for fabricating PP/reduced graphene oxide (rGO) nanocomposites. In the polymerization stage, the synthesized catalyst exhibited a very high activity toward propylene polymerization, while the resultant PP/rGO with a very high isotactic index (I.I. = 99.3), broad molecular weight distribution (M_w/M_n = 14.9), and thermal stability was produced. After melt-blending with commercial PP, a significantly increased modulus along with no observable change in tensile strength and elongation-at-break were achieved via the addition of a very small amount of rGO; these properties resulted from the suitable dispersion and good interface adhesion of the graphene sheet and PP matrix. Thus, this work provides a method for production of high performance PP. **Polyolefins J (2017) 4: 69-77**

Keywords: Polypropylene; nanocomposites; in situ polymerization; graphene

INTRODUCTION

Polypropylene (PP) is one of the most widely used commercial polymers in many applications because of its cost-effectiveness in addition to its intrinsic properties of low density, high stiffness, and good tensile strength[1-3]. However, for advanced applications, physicochemical properties of PP need further improvement. Thus, the study of PP nanocomposites has attracted considerable attention especially regarding nanocomposites containing carbon additives (e.g., graphene and carbon nanotubes) because of their enhanced characteristics such as mechanical properties, thermal stability, flame resistance, and thermal and electrical conductivities[4-8].

Although the dispersion of graphene into polar polymers has been successfully achieved [9-15], the synthesis of graphene-reinforced polymer nanocomposites is challenging and has resulted in well-dispersed graphene fillers for non-polar polyolefin

* Corresponding Author - E-mail: kbyoon@knu.ac.kr

matrices, especially polyolefin products such as polyethylene (PE) and PP. While the performance conferred by these fillers can only be achieved when they are homogeneously dispersed, strong interfacial adhesion between the fillers and polymer matrices has been realized [16,17]. As for preparation of polyolefin-based nanocomposites, several groups have used graphene and graphite prototypes as starting materials because the poor dispersion of fillers (or their weak adhesion) resulted in only a limited degree of physicochemical property improvement[18-20]. For example, Mülhaupt et al.[21] reported a one-step mechanochemical process to prepare polyethylene/ graphene nanocomposites in which the graphene exhibited a markedly improved modulus (only at a high graphene loading (5 wt%)) and losses in elongation-at-break. Similar results obtained for PE/ graphene prepared by a melt compounding method were reported by Wong et al. [22]. The development of polymer nanocomposites must be concerned with maintaining a high level of stiffness-toughness balance because it is the goal of high-performance general plastics for engineering purposes.

Therefore, in this research, we report a facile combination of in situ polymerization and masterbatch method for fabricating one of the most rapidly developing plastic-PP/ reduced graphene oxide (rGO) nanocomposites. This study shows a simplistic technique that can be used to optimize the stiffness-toughness behavior of PP by incorporating a very small amount of rGO sheets.

EXPERIMENTAL

Materials

Expanded graphite (Timcal Graphite & Carbon, Switzerland, <100 μm, 99.9%), H_2SO_4 (95%), HCl (37%), H_2O_2 (28%; Duk San Chemical Co.), sodium nitrate (Dae Jung Co.), n-butylmagnesium chloride (BuMgCl in THF, Sigma-Aldrich) triethylaluminium (TEA, Tosoh Akzo, Japan), titanium tetrachloride ($TiCl_4$, Sigma Aldrich, US), and potassium permanganate (Sigma Aldrich, US, >99.0%) were used as received. Diisobutylphthalate (DIBP) and diethylsuccinate (DS) were purchased from Sigma-Aldrich Co. Cyclohexylmethyldimethoxysilane (C-donor) and dicyclopentyldimethoxysilane (D-donor) were provided by Samsung Total Petrochemicals Co., Ltd., Korea. Polymerization grade propylene and polypropylene (HJ4006) were provided by Korea Petrochemical Ind. Co., Ltd., Korea. n-Hexane and THF were distilled from sodium/ benzophenone under nitrogen prior to use.

Preparation of graphene oxide-supported Ziegler-Natta catalysts

GO was prepared from expanded graphite using the Hummers' oxidation method [23,24]. BuMgCl (1.25 mol) in THF was added dropwise to a THF suspension (1.5 L) containing GO (1.0 g). After the reaction proceeded for 12 h at reflux temperature (80°C), the excess Grignard reagent was filtered, and the solid was subsequently washed with THF and n-hexane five times. The resultant GO/BuMgCl support was suspended in 500 mL n-hexane under ultrasonication for 10 min. Then, the internal donor (DIBP or DS, [Mg]/ [ID] = 8) was added to the suspension. Afterwards, $TiCl_4$ (20 mL) was added dropwise to the suspension of GO/BuMgCl/Donor at 0°C. The temperature was then increased to 80°C, and the mixture was stirred for 4 h. The mixture was filtered to remove the unreacted $TiCl_4$, and a second round of $TiCl_4$ (20 mL) was charged into the reactor. The reaction was completed after stirring for 4 h at 80°C. The reaction mixture was filtered, and the solid was washed several times with hot n-hexane. The resultant powdery product was dried under vacuum at 60°C for 3 h. The GO/ BuMgCl/$TiCl_4$, GO/BuMgCl/DIBP/$TiCl_4$, and GO/ BuMgCl/DS/$TiCl_4$ catalysts were renamed as CAT-1, CAT-2, and CAT-3, respectively.

In situ polymerization and masterbatch method

The polymerization was performed in a 300-mL glass reactor equipped with a magnetic stirring bar. The reactor was back-filled three times with nitrogen and charged with the required amount of n-hexane. At the stipulated temperature, the reaction solution was stirred under 1 atm of propylene for the desired period of time, and then the cocatalyst (TEA) was added to the reactor. After cocatalyst addition, the external donor and catalyst were injected separately, and polymerization with a continuous feed of propylene was started. The propylene pressure was kept constant throughout the polymerization through the use of a bubbler. After 2 h, the polymerization was terminated by adding 10% HCl-methanol solution. The mixture was poured into methanol (500 mL) to precipitate

the polymer and then dried under vacuum at 60°C to constant weight. The resultant PP/GO powders were named as PP/rGO masterbatch. Then, the PP/GO masterbatch was blended with commercial PP using a twin screw mixer (Plasticoder PLE331, Brabender) at 230°C and 100 rpm for 5 min.

Characterization

The Mg and Ti content of the catalyst was determined using inductively coupled plasma atomic emission spectroscopy (ICP, PerkinElmer, Optima 7300DV). The chemical structure of the catalyst was examined using Fourier transform infrared (FTIR) spectroscopy (Jasco 4100, Japan).

The polymer product was fractionated by extraction with boiling n-heptane for 12 h to determine the isotactic index (I.I.). The I.I. values were reported for each sample as the weight percentage of insoluble parts of n-heptane.

The melting temperature (T_m) of the obtained PP was determined using differential scanning calorimetry (DSC, DSC131evo, Setaram) at a heating rate of 10°C/min. The sample was heated to 200°C and held in a molten state for 3 min to eliminate the influence of the thermal history. The PP melt was cooled to 30°C at a rate of 10°C/min. The melting point was determined in the second scan. Decomposition temperature analysis was conducted under a nitrogen atmosphere using a thermogravimetric analyzer (TGA, Setaram Labsys evo) with a programmed heating rate of 10°C/min from 30 to 800°C. The molecular weight and molecular weight distribution (MWD) of PP were determined by high temperature gel permeation chromatography (GPC, PL GPC-220) with 1, 2, 4-trichlorobenzene as the solvent at 135°C. The mechanical properties of the PP and PP/rGO nanocomposites were determined using a universal testing machine (Instron M4465) according to ASTM D882.

RESULTS AND DISCUSSION

The components of the catalysts were evaluated using FTIR spectroscopy to confirm the catalyst structures and to clarify the interactions among the components. The spectra are given in the Supporting Information (Figure S1).

The treatment of GO with BuMgCl can lead to the formation of –O–Mg–Cl groups (1650 cm^{-1}) [25,26]. After treatment with BuMgCl, the C=O stretching vibration at 1720 cm^{-1} and the OH deformation band at 1409 cm^{-1} in GO disappeared. A peak at 1060 cm^{-1} attributed to C–O stretching, which was indicative of a chemical reaction between GO and BuMgCl, was observed.

The structures of the CAT-2 and CAT-3 catalysts were also investigated with FTIR spectroscopy (Figures S2 and S3). A C=O peak for GO/BuMgCl/DIBP and GO/BuMgCl/DS appeared at 1704 cm^{-1} and 1720 cm^{-1} from the MgCl-DIBP and MgCl-DS complexes, respectively[27,28]. After treatment with $TiCl_4$, the carbonyl peak shifted to 1690 cm^{-1}, which indicated interaction between the internal donor and $TiCl_4$.

The GO and GO/BuMgCl were further characterized by Raman analysis, and the spectra are shown in Figure 1. GO displayed a D-band at 1340 cm^{-1} and a G-band at 1580 cm^{-1}. According to Ruoff et al.[29] the D-band is from the structural imperfections created by the attachment of hydroxyl and epoxide groups, whereas the G band represents the sp^2 carbon structures. The D/G intensity ratios increased with the introduction of BuMgCl. This indicated that considerable numbers of small graphitic domains were created because of the BuMgCl treatment. Accordingly, the GO was reduced during the reaction with BuMgCl [30]. The same phenomena were also observed by other researchers

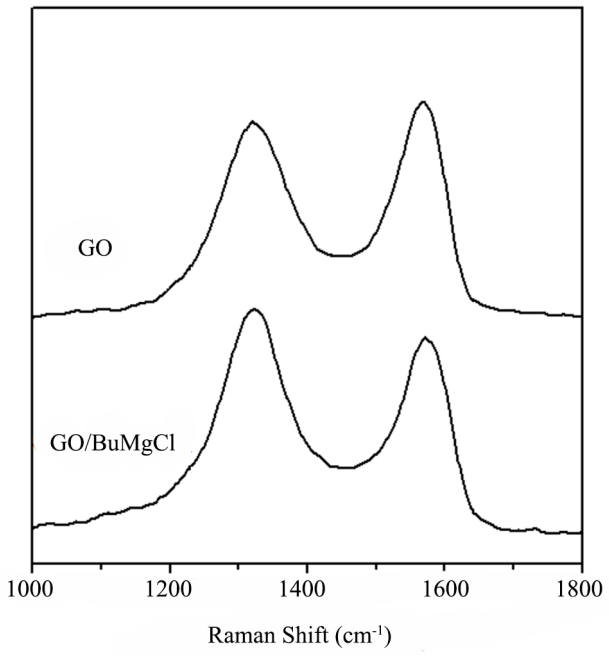

Figure 1. Raman spectra of GO and GO/BuMgCl.

Table 1. Effects of donor (internal donor and external donor) on catalytic performance and properties of the obtained products[(a)].

Catalysts	ED	Activity (kgPP/g Ti.h)	I.I (wt%)	T_m (°C)	T_c (°C)	M_w (×10^{-4}g/mol)	M_w/M_n
CAT-1	-	2.1	66.1	157.3	114.5	11.9	10.9
	C-donor	0.9	92.2	162.0	123.6	26.9	8.4
	D-donor	1.0	91.2	162.2	122.7	22.0	9.2
CAT-2	-	2.5	85.8	158.2	113.4	27.1	14.9
	C-donor	1.3	98.2	159.7	117.7	51.4	7.6
	D-donor	1.4	99.1	161.0	120.1	60.0	11.2
CAT-3	-	2.2	86.7	158.2	117.6	32.6	15.6
	C-donor	1.7	99.3	159.9	120.1	53.0	9.3
	D-donor	1.7	98.3	161.0	120.7	46.4	11.2

[(a)] Polymerization conditions: 40 mg catalyst, [Al]/[Ti] = 200, [ED]/[Al] = 0.1, atmosphere pressure, 40 °C, 2 h

[31]. Therefore, the PP/rGO masterbatch could be directly obtained through an in situ propylene polymerization with the GO/BuMgCl-supported Ti-based catalyst[31].

The performance of the synthesized GO/BuMgCl-supported catalyst for propylene polymerization was evaluated after activation with the TEA cocatalyst in the absence and presence of an external donor. The polymerization results are summarized in Table 1. The catalyst activity of CAT-1, CAT-2, and CAT-3 in the absence of an external donor were 2.1, 2.5, and 2.2 kg/g Ti.h, respectively. After the addition of an external donor (C-donor or D-donor), the catalyst activities drastically decreased. The decreased catalytic activity could be ascribed to the positioning of the non-stereospecific sites of the catalysts [32]. Therefore, the PP obtained in the presence of internal and/or external donors exhibited a very high I.I. value. Interestingly, the I.I. value of PP obtained from CAT-3 in the presence of the C-donor was as high as 99.3 wt%. All of the resultant PP/rGO products were characterized by DSC and GPC. As shown in Table 1, the T_m of the obtained PP was in the range of 157.3–162.2°C and increased upon the addition of an external donor. In addition, the DSC traces were generally smooth curves with relatively sharp endothermic peaks, thus, reflecting the overall homogeneity of the PP. The molecular weight of PP was increased with the introduction of Lewis bases (internal donor and external donor). This phenomenon could correspond to the introduction of external donor leading to an increase in isotactic PP yield, as it is well known that the isotactic polymer has a higher molecular weight than atactic polymer in the heterogeneous Ziegler-Natta catalyst system [32-35]. The molecular weight distribution (M_w/M_n) of PP was significantly influenced by the structure of the internal and/or external donors. In this work, the M_w/M_n of PP was in the range of 7.6 to 15.6, which was influenced by changing the internal and external donors (Figure 2).

In Figure 3, the XRD patterns of GO, PP/rGO

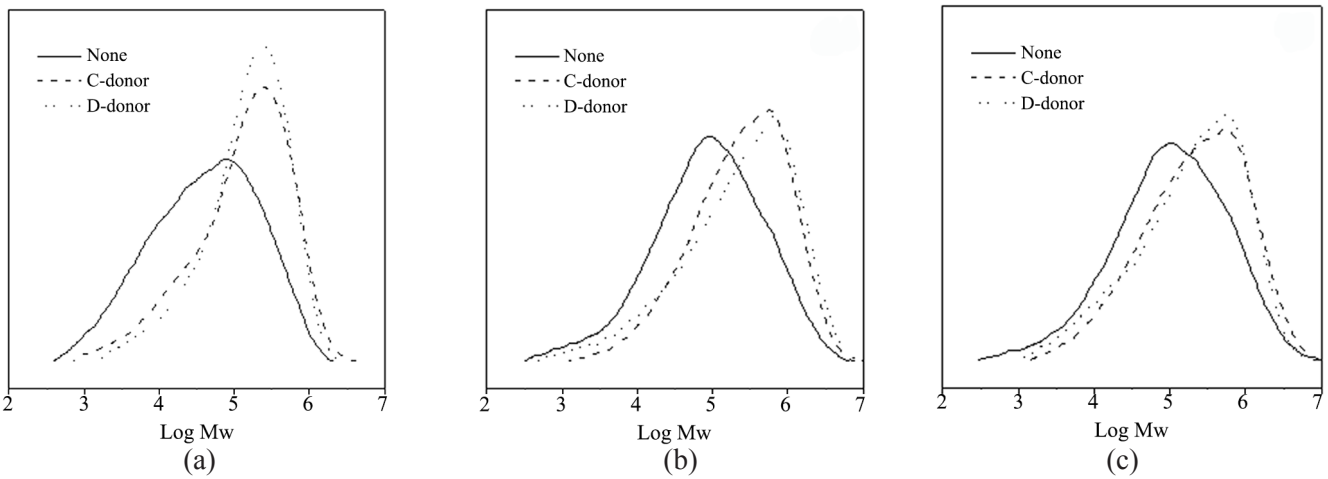

Figure 2. GPC curves of PP obtained with (a) CAT-1, (b) CAT-2 and (c) CAT-3.

Table 2. Thermal and mechanical properties of PP nanocomposites at various filler content.

Sample	GO, TEG content (wt%)	T_m (°C)	T_c (°C)	Modulus (MPa)	Tensile strength (MPa)	Elongation-at-break (%)
PP	-	162.4	119.4	180±30	32±3	1040±100
PP-rGO0.1	0.1	163.7	120.7	230±30	33±3	600±100
PP-rGO0.2	0.2	164.4	125.8	230±30	32±3	1030±200
PP-rGO0.5	0.5	165.4	127.2	230±30	33±3	1050±200
PP-rGO1.0	1.0	162.7	122.0	230±30	32±3	1030±200
PP-TEG0.1	0.1	163.4	122.0	200±50	35±3	20±5
PP-TEG0.5	0.5	164.0	123.1	225±50	34±3	15±5
PP-TEG1.0	1.0	163.6	124.2	245±50	32±3	15±5

masterbatch that obtained from CAT-2 in the presence of D-donor and PP are compared. The XRD pattern of GO shows a broad, tall peak at approximately 12.1º, which is the characteristic peak of GO, corresponding to a d-spacing of approximately 0.73 nm. The larger interlayer spacing than that of graphite (~0.34 nm) is attributable to the presence of functional groups. It was also found that PP and PP/rGO masterbatch are characterized by diffraction peaks at 2θ =14.1°, 16.9°, 18.5°, 21.3°, and 21.9° associated with the (110), (040), (130), (111), and (041) reflections. No conspicuous diffraction peaks are observed except the crystalline diffraction peaks of the PP matrix, indicating that no significant stacking of GO sheets occurs in PP/rGO masterbatch.

The PP/rGO masterbatch obtained from CAT-2 in the presence of the D-donor was subsequently melt blended with commercial PP to fabricate the PP/rGO nanocoposites with different rGO loadings.

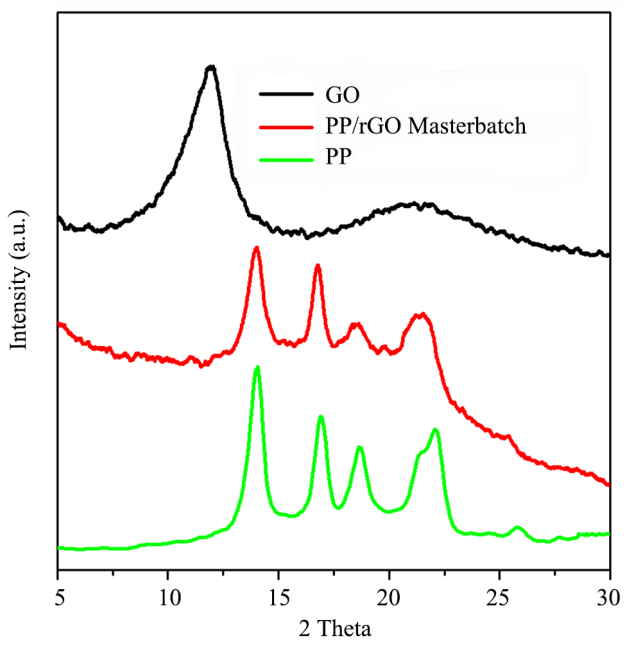

Figure 3. XRD curves of GO, PP/rGO masterbatch and PP.

For comparison, PP nanocomposites containing dispersed thermally expanded graphite (TEG) were prepared by melt mixing too. The effect of rGO and TEG on the crystallization of PP was investigated by DSC. As shown in Table 2, the T_m of pristine PP was 162.4°C. With the introduction of rGO or TEG, the T_m increased. Additionally, compared with neat PP, the non-isothermal crystallization peak temperature (T_c) increased with the addition of rGO or TEG, which demonstrated that the rGO and TEG nanoplatelets could act as nucleating agents. The crystallinity of PP and its nanocomposites were also calculated by DSC. Upon increase in graphene content, a slightly increase in the crystallinity of PP was observed. Fu et al. [36] also observed the same phenomenon for PP/exfoliated graphene nanocomposites.

The mechanical properties of the prepared PP-based nanocomposites were examined at room temperature. Figure 4 shows the relationship between the nanocomposite mechanical properties and the rGO content. The addition of even small amounts of rGO to the PP matrix significantly improved the mechanical properties. The addition of only 0.1 wt% GO resulted in an increase in the modulus of about 30% compared with that of commercial PP without a tensile strength reduction. This increase in the modulus was attributed to the reinforcement of the nanocomposite by the rGO sheets. Compared with commercial PP, all of the PP/rGO nanocomposites in which the GO was well dispersed showed clear increases. Upon dispersion of 1.0 wt% rGO into PP, the PP/rGO nanocomposites were black in color and completely opaque, whereas the PP/rGO samples were light gray at the lowest rGO content of 0.1 wt%. With regard to the rGO content greater than 0.2 wt%, the modulus of the commercial PP was improved approximately 30% with almost no change in tensile strength and elongation-at-break. For the results of the

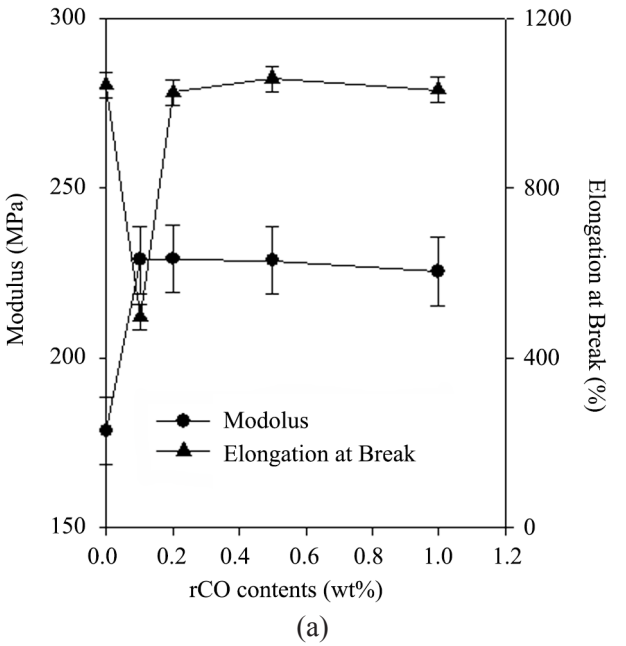

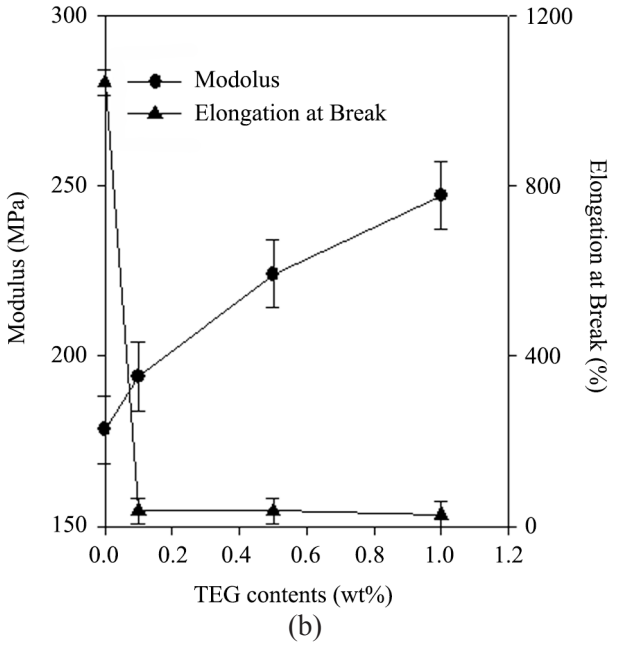

Figure 4. Modulus and elongation-at-break of the (a) PP/ rGO and (b) PP/TEG nanocomposites.

PP/TEG samples, although the modulus and tensile strength were improved with the introduction of TEG, the elongation-at-break drastically reduced to <2% of the original PP value. The above results indicated that the PP/rGO nanocomposites obtained by the combined in situ polymerization with masterbatch method had a remarkable stiffness-toughness balance. We suggested that the excellent physical properties could be dependent on the suitable dispersion and strong interfacial adhesion between the rGO and PP matrix.

Table 3. Thermal stabilities of PP and PP/rGO nanocomposites at various rGO content.

Sample	rGO content (wt%)	Weight loss (5 wt%, °C)	Char yield (wt%)
PP	-	369.3	0.0
PP/rGO Masterbatch	3.2	433.8	7.8
PP-rGO0.1	0.1	412.7	3.2
PP-rGO0.2	0.2	418.4	4.7
PP-rGO0.5	0.5	420.7	5.9
PP-rGO1.0	1.0	423.1	7.6

The thermal stability of a polymeric material is important because it is often the limiting factor in both processing and end-use applications. The thermal degradation of PP and PP/rGO nanocomposites with different weight fractions of rGO was determined from their weight losses during heating under a nitrogen atmosphere. The temperatures for 5% weight losses (T_d5%) and the char yields (%) were obtained from the data presented in Figure 5, and the results are summarized in Table 3. All of the TGA curves exhibited a single degradation. The degradation temperature at 5 wt% loss of the PP/rGO nanocomposites was 412.7°C, 418.4°C, 420.7°C, and 423.1°C for 0.1 wt%, 0.2 wt%, 0.5 wt%, and 1.0 wt% rGO, respectively. Though the degradation temperature at 5 wt% loss of the commercial PP and PP/rGO masterbatch was 369.3°C and 433.8 °C, respectively. The improvement in thermal stability of PP in the presence of rGO was attributed to the great

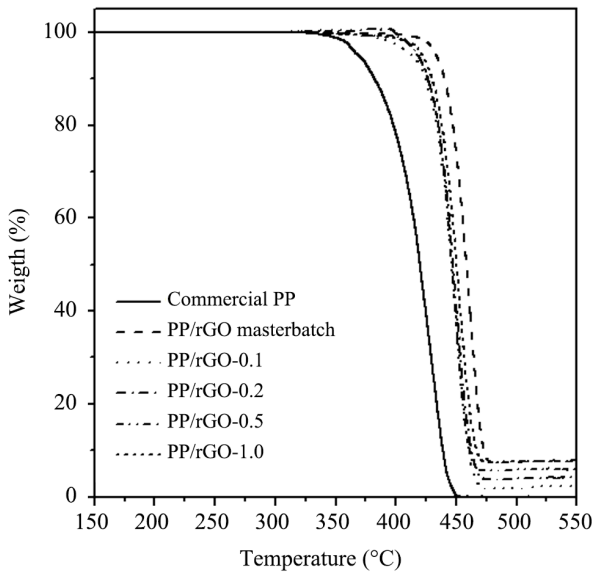

Figure 5. TGA curves of the PP/rGO nanocomposites at various rGO content.

dispersion of rGO in the PP matrix, which may act as an insulator between the heat source and the surface area of the polymer where the combustion occurs. Additionally, the rGO layers may have hindered the diffusion of volatile decomposition products within the PP/rGO nanocomposites by promoting char formation [36,37]. As shown in Figure 5, the char yield of PP and PP/rGO nanocomposites with 0.1 wt%, 0.2 wt%, 0.5 wt%, and 1.0 wt% rGO was 3.2 wt%, 4.7 wt%, 5.9 wt%, and 7.6 wt%, respectively. The char-formed layer could have acted as a mass transport barrier that retarded the escape of the volatile products generated as the PP decomposed [38,39]. Therefore, the char yields of the nanocoposites increased with an increase of rGO because the rGO in the PP matrix promoted carbonization on the polymer surface. Furthermore, unburned filler and the high heat resistance exerted by the filler itself also contributed to higher char residues.

CONCLUSION

PP with a very high isotactic index (I.I. = 99.3) and broad molecular weight distribution (M_w/M_n = 14.9) was successfully obtained through in situ propylene polymerization with a GO/BuMgCl-supported Ti-based Ziegler-Natta catalyst. The resultant products were used as a masterbatch to reinforce the commercial PP through a melting blending method. The obtained PP/rGO nanocomposites exhibited a significant improvement in modulus with almost no changes in tensile strength and elongation-at-break at a very small amount of rGO loading. Thus, this work provides a facile method for production of high performance PP with a stiffness-toughness balance.

ACKNOWLEDGEMENTS

This research was supported by Kyungpook National University Research Fund, 2016. The authors would also like to acknowledge the financial support from National Natural Science Foundation of China (No. U1462124). Dr. H.X. Zhang would like to thank the China Scholarship Council (201504910334) for the financial support on his visit at KNU.

REFERENCES

1. Kissin YV (2008) Alkene polymerization reactions with transition Metal catalysts, Elsevier, Amsterdam
2. Vasile C (2000) Handbook of polyolefins, Marcel Dekker, New York
3. Bahri-Laleh N, Nekoomanesh M, Sadjadi S, Pajouhan A (2016) Polyolefin and olefin production in Iran: Current and future capacities, Polyolefin J 3: 11-22
4. Ameli A, Nofar M, Park CB, Pötschke P, Rizvi G (2014) Polypropylene/carbon nanotube nano/microcellular structures with high dielectric permittivity, low dielectric loss, and low percolation threshold. Carbon 71: 206-217
5. Yuan B, Bao C, Song L, Hong N, Liew KM, Hu Y (2014) Preparation of functionalized graphene oxide/polypropylene nanocomposite with significantly improved thermal stability and studies on the crystallization behavior and mechanical properties. Chem Eng J 237: 411-420
6. Molavi FK, Soltani S, Naderi G, Bagheri R (2016) Effect of multi-walled carbon nanotube on mechanical and rheological properties of silane modified EPDM rubber, Polyolefin J 3: 69-77
7. Zhou G, Li L, Wang DW, Shan XY, Pei S, Li F, Cheng HM (2015) A Flexible Sulfur graphene polypropylene separator integrated electrode for advanced Li-S batteries, Adv Mater 27: 641-647
8. Prashantha K, Soulestin J, Lacrampe MF, Krawczak P (2014) Processing and characterization of polypropylene filled with multiwalled carbon nanotube and clay hybrid nanocomposites. Int J Polym Anal Char 19: 363-371
9. Ramanathan T, Abdala AA, Stankovich S, Dikin DA, Herrera-alonso M, Pinter RD, Adamson DH, Schniepp HC, Chen X, Ruoff RS, Nguyen ST, Aksay IA, Prud'Homme RK Brinson LC (2008) Functionalized graphene sheets for polymer nanocomposites. Nat Nanotechnol 3: 327-331
10. Kim H, Macosko CW (2008) Morphology and properties of polyester/exfoliated graphite nanocomposites, Macromolecules 41: 3317-3327
11. Debelak B, Lafdi K (2007) Use of exfoliated

graphite filler to enhance polymer physical properties. Carbon 45: 1727-1734
12. Rafiee MA, Rafiee J, Wang Z, Song HH, Yu ZZ, Koratkar N (2009) Enhanced mechanical properties of nanocomposites at low graphene content. ACS Nano 3: 3884-3890
13. Raghu AV, Lee YR, Jeong HM, Shin CM (2008) Preparation and physical properties of waterborne polyurethane/functionalized graphene sheet nanocomposites. Macromol Chem Phys 209: 2487-2493
14. Lee YR, Raghu AV, Jeong HM, Kim BK (2009) Properties of waterborne polyurethane/ functionalized graphene sheet nanocomposites prepared by an in situ method. Macromol Chem Phys 210: 1247-1254
15. Xu YX, Hong WJ, Bai H, Li C, Shi GQ (2009) Strong and ductile poly(vinyl alcohol)/graphene oxide composite films with a layered structure. Carbon 47: 3538-2543
16. Camargo PHC, Satyanarayana KG, Wypych F (2009) Nanocomposites: Synthesis, structure, properties and new application opportunities. Mat Res 12: 1-39
17. Pavlidou S, Papaspyrides CD (2008) A review on polymer-layered silicate nanocomposites. Prog Polym Sci 33: 1119-1198
18. Fu S, Li N, Wang K, Zhang Q, Fu Q (2015) Reduction of graphene oxide with the presence of polypropylene micro-latex for facile preparation of polypropylene/graphene nanosheet composites. Colloid Polym Sci 293: 1495-1503
19. Ryu SH, Shanmugharaj AM (2014) Influence of hexamethylene diamine functionalized graphene oxide on the melt crystallization and properties of polypropylene nanocomposites. Mater Chem Phys 146: 478-486
20. Vallés C, Abdelkader AM, Young RJ, Kinloch IA (2014) Few layer graphene–polypropylene nanocomposites: The role of flake diameter. Faraday Discuss 173: 379-390
21. Beckert F, Bodendorfer S, Zhang W, Thomann R, Mulhaupt R (2014) Novel graphene UHMWPE nanocomposites prepared by polymerization filling using single-site catalysts supported on functionalized graphene nanosheet dispersions. Macromolecules 47: 7036-7042
22. Zheng W, Lu X, Wong SC (2004) Electrical and mechanical properties of expanded graphite-reinforced high-density polyethylene. J Appl Polym Sci 91: 2781-2788
23. Hummers Jr WS, Offeman RE (1958) Preparation of graphitic oxide. J Am Chem Soc 80: 1339-1339
24. Perera SD, Mariano RG, Vu K, Nour N, Seitz O, Chabal Y, Balkus Jr KJ (2012) Hydrothermal synthesis of graphene-TiO_2 nanotube composites with enhanced photocatalytic activity. ACS Catalysis 2: 949-956
25. Munoz-Escalona A, Fuentes A, Liscano J, Albornoz A (1990) High active Ziegler-Natta catalysts for homo- and copolymerization of ethylene by supporting a grignard compound and $TiCl_4$ on SiO_2. In: Studies in surface science and catalysis, T Keii, K Soga (Eds.), Kodansha, Tokyo, 377-404
26. Nowlin E, Kissin YV, Wagner KP (1988) High activity Ziegler–Natta catalysts for the preparation of ethylene copolymers. J Polym Sci Pol Chem 26: 755-764
27. Chien JCW, Wu JC, Kuo CI (1983) Magnesium chloride supported high-mileage catalysts for olefin polymerization. IV. FTIR and quantitative analysis of modifiers in the catalysts, J Polym Sci Pol Chem 21: 725-736
28. Spitz R, Lacombe JL, Guyot A (1984) Catalyseurs Ziegler-Natta supportés sur $MgCl_2$ pour la polymérisation stéréorégulée du propène. III. Systèmes catalytiques à hautes performances comprenant un solide ternaire: $MgCl_2$, ester aromatique, $TiCl_4$. J Polym Sci Pol Chem 22: 2641-2650
29. Yang D, Velamakanni A, Bozoklu G, Park S, Stoller M, Piner RD, Stankovich S, Jung I, Field DA, Ventrice Jr CA, Ruoff RS (2009) Chemical analysis of graphene oxide films after heat and chemical treatments by X-ray photoelectron and micro-Raman spectroscopy. Carbon 47: 145-152
30. Wang H, Robinson JT, Li X, Dai H (2009) Solvothermal reduction of chemically exfoliated graphene sheets. J Am Chem Soc 131: 9910-9911
31. Huang Y, Qin Y, Wang N, Zhou Y, Niu H, Dong JY, Hu J, Wang Y (2012) Reduction of graphite oxide with a Grignard reagent for facile in situ preparation of electrically conductive polyolefin/ graphene nanocomposites. Macromol Chem Phys 213: 720-728

32. Zhang HX, Lee YJ, Park JR, Lee DH, Yoon KB (2011) Control of molecular weight distribution for polypropylene obtained by commercial Ziegler-Natta catalyst: Effect of electron donor. Macromol Res 19: 622-628
33. Sacchi MC, Forlini F, Tritto I, Mendichi R, Zannoni G, Noristi L (1992) Activation effect of alkoxysilanes as external donors in magnesium chloride-supported Ziegler-Natta catalysts. Macromolecules 25: 5914-5918
34. Kakugo M, Miyatake T, Naito Y, Mizunuma K (1988) Microtacticity distribution of polypropylenes prepared with heterogeneous Ziegler-Natta catalysts. Macromolecules 21: 314-319
35. Zhang HX, Shin YJ, Lee DH, Yoon KB (2011) Preparation of ultra-high molecular weight polyethylene with $MgCl_2/TiCl_4$ catalyst: Effect of internal and external donor on molecular weight and molecular weight distribution. Polym Bull 66: 627-635
36. Song P, Cao Z, Cai Y, Zhao L, Fang Z, Fu S (2011) Fabrication of exfoliated graphene-based polypropylene nanocomposites with enhanced mechanical and thermal properties. Polymer 52: 4001-4010
37. Milani MA, González D, Quijada R, Basso NRS, Cerrada ML, Azambuja DS, Galland GB (2013) Polypropylene/graphene nanosheet nanocomposites by in situ polymerization: Synthesis, characterization and fundamental properties. Compos Sci Technol 84: 1-7
38. Bao C, Guo Y, Song L, Hu Y (2011) Poly(vinyl alcohol) nanocomposites based on graphene and graphite oxide: A comparative investigation of property and mechanism. J Mater Chem 21: 13942-13950
39. Goncalves G, Marques PAAP, Barros-Timmons A, Bdkin I, Singh MK, Emami N, Gracio J (2010) Graphene oxide modified with PMMA via ATRP as a reinforcement filler. J Mater Chem, 20: 9927-9934